Chemical Physics Letters 551 (2012) 1–6

Contents lists available at SciVerse ScienceDirect

Chemical Physics Letters

journal homepage: www.elsevier.com/locate/cplett

FRONTIERS ARTICLE

Sub-Doppler mid-infrared spectroscopy of molecular ions

Kyle N. Crabtree [a,1], James N. Hodges [a], Brian M. Siller [a], Adam J. Perry [a], Joseph E. Kelly [a], Paul A. Jenkins II [a], Benjamin J. McCall [a,b,*]

[a] Department of Chemistry, University of Illinois, Urbana, IL 61801, USA
[b] Departments of Astronomy and Physics, University of Illinois, Urbana, IL 61801, USA

ARTICLE INFO

Article history:
Available online 15 September 2012

ABSTRACT

The technique of velocity modulation spectroscopy has recently been combined with cavity enhancement and frequency modulation methods into a technique called noise-immune cavity-enhanced optical heterodyne velocity modulation spectroscopy (NICE-OHVMS). We have implemented NICE-OHVMS with a cw-optical parametric oscillator (OPO) tunable from 3.2 to 3.9 μm, and used it to record spectra of the $R(1,0)$ and $R(1,1)^u$ transitions of the v_2 fundamental band of H_3^+. The high optical power and cavity enhancement enable saturation of rovibrational transitions, which allows for line center frequencies to be measured with a precision of 70 kHz.

1. Introduction

Molecular ions play a key role as intermediates in chemical reactions, and a detailed understanding of their structure and intramolecular dynamics in the gas phase, generally obtained by spectroscopy, is a critical first step toward understanding their behavior in more complicated systems. The primary technique used for ion spectroscopy over the past 30 years has been velocity modulation spectroscopy (VMS) [1,2]. In VMS, ions are produced in an AC positive column plasma whose polarity is alternated at frequency f_{vm}. The average drift velocity of the ions in the plasma is shifted toward the cathode from the applied electric field, while neutral molecules are generally unaffected. As the polarity is reversed, the average ion drift velocity also reverses, resulting in a periodic oscillation in the ion velocity distribution at f_{vm}. By interrogating the ions with a laser beam passing in one direction through the plasma, the absorption profiles are alternately red- and blue-shifted with respect to their rest frequencies, and phase-sensitive detection at f_{vm} allows for selective retrieval of ionic signals. VMS therefore addresses one of the main challenges of ion spectroscopy, i.e., detection of ionic species that are only $\sim 10^{-5}$–10^{-6} as abundant as neutral molecules. Well over 40 unique molecular ions (not including isotopologues) have been detected with VMS; these have been extensively reviewed by Stephenson and Saykally [3].

Recently, the use of a Fabry–Perot optical cavity to enhance the optical path length was demonstrated by Siller et al. (cavity-enhanced velocity modulation spectroscopy, CEVMS), who locked a Ti:Sapphire laser to an optical cavity surrounding a velocity modulated positive column cell and detected the transmitted light [4]. Because the light in the cavity is bidirectional, red and blue Doppler shifts are simultaneously superimposed, encoding the velocity modulation (VM) signal at $2f_{vm}$. Initially, this was believed to be problematic because any neutral molecules produced or excited by the discharge are concentration modulated (CM) at $2f_{vm}$; that is, the population of the excited species varies with the magnitude of the applied voltage, but not the sign of the voltage. By also encoding the ion signal at $2f_{vm}$, it was thought the concentration modulation signal of neutral molecules would overwhelm the ion velocity modulation signal. Siller et al. showed that the ion and neutral signals occurred at different phases with respect to the plasma voltage, thereby preserving ion-neutral discrimination through phase-sensitive detection. Additionally, the power enhancement from the optical cavity enables saturation spectroscopy and precise line-center determination [5]. A related technique has also been employed using an optical frequency comb as the light source and a unidirectional ring cavity surrounding a plasma cell, effectively converting VMS to a broadband technique while preserving the high resolution of laser spectroscopy [6].

Cavity enhanced absorption spectroscopy suffers from the fact that frequency noise in the laser is directly converted into intensity noise as a result of reduced cavity transmission. This limitation was overcome by Ye et al. with noise-immune cavity-enhanced

* Corresponding author at: Department of Chemistry, University of Illinois, Urbana, IL 61801, USA.
E-mail addresses: kcrabtr2@illinois.edu (K.N. Crabtree), jnhodge@illinois.edu (J.N. Hodges), bsiller2@illinois.edu (B.M. Siller), aperry10@illinois.edu (A.J. Perry), bjmccall@illinois.edu (B.J. McCall).
URL: http://bjm.scs.illinois.edu (B.J. McCall).
[1] Present address: Harvard-Smithsonian Center for Astrophysics, Cambridge, MA 02138, USA.

0009-2614/$ - see front matter © 2012 Elsevier B.V. All rights reserved.
http://dx.doi.org/10.1016/j.cplett.2012.09.015

optical heterodyne molecular spectroscopy (NICE-OHMS) [7]. In this technique, the laser is phase modulated at f_h (typically ~100s of MHz), effectively generating an FM triplet consisting of a carrier (at the optical frequency f_o) and a pair of sidebands with opposite phase at $f_o \pm f_h$. The triplet is coupled into the optical cavity by setting f_h equal to an integer multiple of the cavity free spectral range (FSR). In the absence of any intracavity absorption or dispersion, the beat notes between each sideband beating with the carrier are balanced in both amplitude and phase, so there is no net signal at f_h. However, in the presence of an intracavity absorber or disperser, the beat notes are unbalanced in amplitude and/or phase, yielding a net signal. By encoding absorption/dispersion information at a high frequency, $1/f$ technical noise is reduced. Another advantage is that any laser frequency noise affects the cavity coupling efficiency of the carrier and both sidebands equally, which keeps the beat notes of each sideband with the carrier balanced, and eliminates direct conversion of laser frequency noise to noise in the final spectrum. The disadvantages are the complexity of the technique, particularly the demands of maintaining the laser-cavity lock, and the requirement of a detector whose bandwidth is at least f_h. An extensive review of the NICE-OHMS technique has been published by Foltynowicz et al. [8].

CEVMS and NICE-OHMS have been combined into a technique called noise-immune cavity enhanced optical heterodyne velocity modulation spectroscopy (NICE-OHVMS) in the near-infrared with a Ti:Sapphire laser [9]. Because f_h and f_{vm} are at significantly different frequencies (typically ~100 MHz and ~10 kHz, respectively), the detector signal is first demodulated at f_h, and then sent on to further phase-sensitive detection at $2f_{vm}$. NICE-OHVMS preserves the ion-neutral discrimination afforded by VMS, and takes advantage of the ultra-high sensitivity, saturation, and noise immunity of NICE-OHMS.

However, the technical demands of the NICE-OHMS technique have largely precluded its use in the mid-infrared spectral region in which VMS has been successfully exploited. The high bandwidth detectors and phase modulators required for NICE-OHMS are not as readily available in the mid-IR compared with the visible/near-IR. The only published mid-IR NICE-OHMS work was done with a quantum cascade laser near 8.5 μm, and was limited by the detector bandwidth and the phase modulation characteristics of the device [10]. Work is currently underway in our laboratory to extend NICE-OHMS into the mid-IR using a difference frequency generation (DFG) source in the 3–5 μm region [11], which is particularly attractive for a general-purpose ion spectrometer because the vast majority of molecules have at least one fundamental vibrational band in that portion of the spectrum.

Here we report the first mid-IR NICE-OHVMS spectrometer, which uses a commercially available cw-optical parametric oscillator (OPO) tunable from 3.2 to 3.9 μm. The high optical power of the OPO (~1 W) allows for use of high bandwidth mid-IR detectors that are not sensitive enough to be used with many other lower-power cw lasers in this region. This technique enables all of the advantages of the NICE-OHVMS technique to be brought to bear on fundamental vibrational transitions of molecular ions, including high precision sub-Doppler spectroscopy.

Our initial demonstration of this instrument focuses on the study of H_3^+, which is the simplest polyatomic molecular ion and serves as the primary initiator of ion–molecule chemistry in interstellar clouds [12,13]. Its infrared spectrum was first observed by Oka in 1980 [14], and since then it has been extensively studied spectroscopically (see, for instance, the review in Ref. [15]). More recent research on H_3^+ focuses on spectroscopy above the so-called "barrier to linearity," at which point the molecule adopts a linear geometry that induces a singularity in the Hamiltonian, complicating its theoretical treatment [16]. Nevertheless, for the lowest-lying energy levels, the agreement between experiment and ab initio theory is good to spectroscopic accuracy [17]. Measuring the energy level spacings experimentally with higher precision and accuracy would present a greater challenge for ab initio theory, possibly spurring new developments. The NICE-OHVMS technique opens the possibility of measuring such energy level spacings in H_3^+.

As a demonstration of the capabilities of this instrument, we present in this Letter spectra of the ν_2 fundamental band of H_3^+ at 3.67 μm. In Section 2 we describe the instrumental details, and in Section 3 we discuss NICE-OHVMS lineshapes and present spectra acquired with the instrument. Finally, in Section 4, the performance of the instrument is assessed, and future directions are discussed.

2. Experimental details

Our NICE-OHVMS instrument is outlined in Figure 1. A Ytterbium-doped fiber laser (YDFL, Koheras Adjustik Y-10) is sent through a fiber EOM (EOSPACE PM-0K5–00-PFU-PFU-106-S), amplified (IPG Photonics YAR-10 K-1064-LP-SF), and used to pump a singly-resonant OPO (Aculight Argos 2400 SF). The pump (1.064 μm) and signal (1.5–1.6 μm) beams are sent to a wavemeter (Burleigh WA-1500) for frequency calibration. The idler (3.2–3.9 μm) is locked with the Pound-Drever-Hall (PDH) technique to a 1.9-m-long optical cavity consisting of two 1 m radius of curvature concave Si mirrors dielectric coated for 99.7% reflectivity over 3.1–3.4 μm surrounding a plasma cell. Cavity reflection and transmission are monitored by photodiodes (Boston Electronics Vigo PVM-10.6-1x1) with an effective bandwidth of ~125 MHz.

Heterodyne and PDH sidebands are generated by applying voltages at their respective frequencies to the fiber EOM on the seed laser simultaneously. The resultant frequency spectrum of the pump laser is imprinted on the idler beam. A PDH error signal used for cavity locking is generated by demodulating the cavity reflection signal at the frequency RF1 (typically 2–20 MHz). The error signal is sent to feedback electronics which stabilize the length of the cavity on slow timescales via a piezoelectric transducer (PZT) attached to one of the cavity mirrors, and apply fast corrections to the idler frequency by a PZT mounted to one of the signal cavity mirrors inside the OPO head. The cavity transmission detector signal is sent to a pair of mixers ~90° out of phase with one another, and each is demodulated at frequency RF2 (equal to the cavity FSR of 79.12 MHz). The overall phase of the heterodyne detection is adjusted by phase shifting the RF signal driving the EOM using cables of appropriate lengths. The demodulated signal from each mixer is then sent to a lock-in amplifier referenced to twice the frequency used to drive the plasma, and the in-phase and quadrature outputs of each amplifier are digitized and stored on a computer.

Ions are produced in a liquid-nitrogen-cooled multi-inlet multi-outlet positive column discharge cell, which is placed between the two free-standing mirrors of the optical cavity [18]. Intracavity radiation is admitted into the cell by means of CaF_2 windows aligned at Brewster's angle. The plasma is driven by a 40 kHz sine wave voltage produced by amplifying the output of an arbitrary waveform generator with an audio amplifier (Techron 7780) and a step-up transformer. H_3^+ was produced at a pressure of 200 mTorr and a discharge current of 170 mA. The outputs of the two mixers were each demodulated at 80 kHz with a lock-in amplifier set to a 10 ms time constant (16 Hz detection bandwidth).

Typical operation begins by filling the cooling jacket of the cell with liquid nitrogen and igniting the plasma. The cavity length is adjusted to bring it into resonance with the laser, and the laser-cavity lock is established. The idler frequency is tuned by applying a voltage to an internal PZT on the YDFL, and the cavity length is

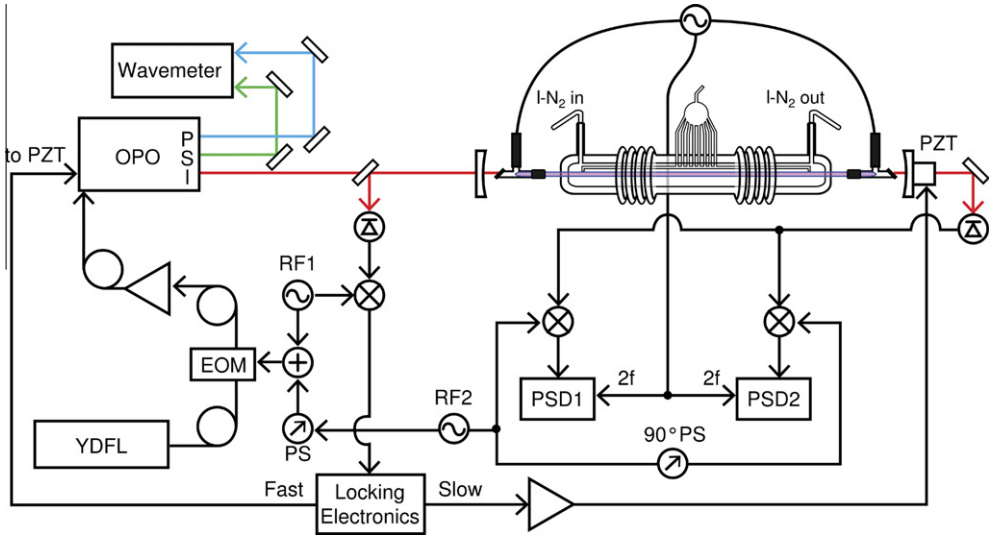

Figure 1. Block diagram of NICE-OHVMS instrument. Details of its operation are given in the main text. YDFL: Ytterbium-doped fiber laser; EOM: electro-optic modulator; OPO: optical parametric oscillator with pump (P, blue), signal (S, green) and idler (I, red) beams; PZT: piezoelectric transducer, PS: phase shifter; PSD: phase sensitive detector; •: signal splitter.

controlled with the locking electronics to maintain the resonance condition. When the cavity PZT reaches the end of its travel, the laser-cavity lock is electronically interrupted, the cavity length is reset to the other end of its travel, a new resonance is found, and the lock is reestablished. In this manner, the spectrometer can scan without manual intervention over the entire range of the YDFL PZT (around 100 GHz), although in practice a scan is generally much shorter. It is in principle possible to extend the automated tuning range further by electronic control of the intracavity etalon of the OPO and the nonlinear crystal position/temperature, but the practical utility of such efforts would likely be minimal.

3. Results and analysis

3.1. Lineshapes

The overall Doppler lineshape for NICE-OHVMS in both absorption and dispersion has odd symmetry, and qualitatively appears similar to the third derivative of a Gaussian absorption profile. A detailed analysis of the lineshape is beyond the scope of this Letter and will be the subject of a future work, but a qualitative description follows. Consider a general NICE-OHMS lineshape such as that shown in panels a and b of Figure 2 in Ref. [8]. If the signal belongs to an ion, then the AC voltage of the plasma causes velocity modulation (VM), Doppler shifting the lineshape at the plasma frequency. As a result of the bidirectional nature of light in our optical cavity, the lineshape is simultaneously Doppler shifted to the red and to the blue by the same amount at each point in time along the plasma voltage cycle. Consequently, the time-dependent signal repeats itself every plasma half-cycle, or at twice the AC plasma frequency ($2f_{vm}$). In addition to VM, an ion also experiences concentration modulation (CM) at $2f_{vm}$, and CM may be phase shifted with respect to VM. Thus, in addition to a periodic Doppler shift at $2f_{vm}$ from VM, the lineshape amplitude varies at $2f_{vm}$ from CM. The net signal observed comes in 4 channels corresponding to the even and odd second order Fourier coefficients of the absorption and dispersion profiles affected by VM and CM.

The sub-Doppler lineshape is more straightforward. As has been discussed in regard to previous NICE-OHMS setups [19,20,9], the carrier and sidebands can each act as pumps and probes for saturation spectroscopy. The Lamb dips arising from the Bennet holes burned in the population appear at half-integer multiples of the carrier-sideband spacing f_h, i.e., at all frequencies at which forward- and reverse-propagating beams sample the same velocity component of the Doppler distribution. At the line center ν_0, when the

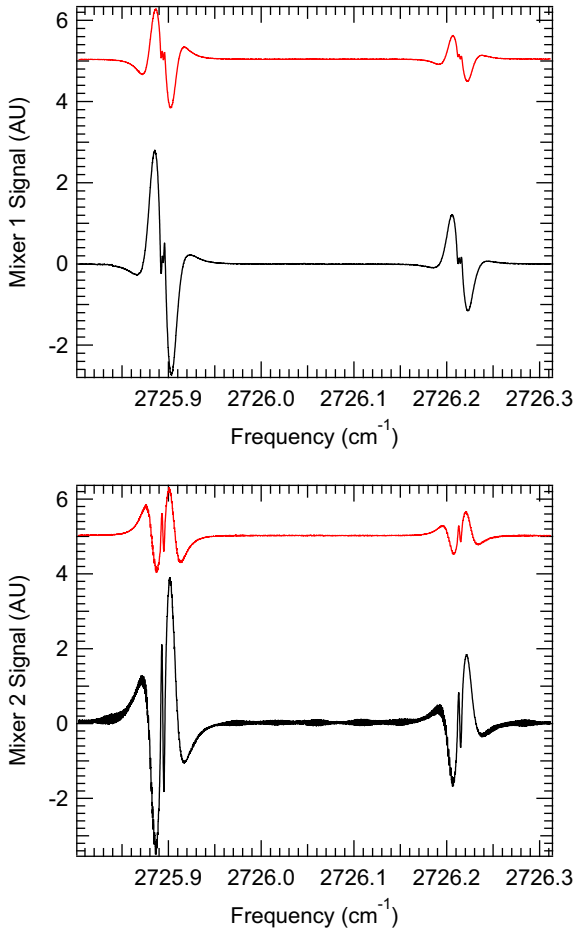

Figure 2. NICE-OHVMS spectrum of the $R(1,0)$ and $R(1,1)^u$ transitions of the ν_2 fundamental band of H_3^+. Each panel shows the in-phase (black, bottom) and quadrature (red, top) outputs of a lock-in amplifier demodulating the indicated mixer's signal.

zero-velocity distribution is both pumped and probed by the carrier, a signal only appears in dispersion as the heterodyne detection scheme employed by NICE-OHMS is insensitive to absorption of the carrier. In the current work, the heterodyne modulation index (β) is small enough ($\sim$0.63) that only the carrier has sufficient power to saturate transitions, while the sidebands can only act as probes. The dispersion signal therefore contains Lamb dips at ν_0 and $\nu_0 \pm f_h/2$, while the absorption signal contains them at $\nu_0 \pm f_h/2$.

While VM and CM have a strong influence on the lineshape of the Doppler profile, they do not affect the sub-Doppler features in the same way. Because Bennet holes are only burned in the population at or spaced evenly around the zero-velocity component of the ion distribution, VM effectively changes the abundance of ions with the appropriate velocity. In that way, VM effectively behaves like CM, and the net effect is to influence the amplitude of the Lamb dip lineshape and the relationship between the amplitudes of the even and odd Fourier coefficients within absorption or dispersion. Neglecting any change of the ions' collision rate with changing velocity, VM and CM do not affect the sub-Doppler profile beyond its amplitude. The sub-Doppler lineshape function [9] is

$$\chi(\nu_d) = \left(A_1\left[\chi_a\left(\nu_d - \frac{f_h}{2}\right) - \chi_a\left(\nu_d + \frac{f_h}{2}\right)\right]\right)\sin\theta_h + \left(-2A_0\chi_d(\nu_d) + A_1\left[\chi_d\left(\nu_d - \frac{f_h}{2}\right) + \chi_d\left(\nu_d + \frac{f_h}{2}\right)\right]\right)\cos\theta_h, \quad (1)$$

where ν_d is the frequency detuning from the transition center frequency, θ_h is the heterodyne detection phase, A_0 is the effective amplitude of the central (carrier-carrier) dispersion Lamb dip, and A_1 is the effective amplitude of the carrier-sideband Lamb dips for absorption and dispersion. $\chi_a(\omega)$ is a Lorentzian lineshape function for absorption, and $\chi_d(\omega)$ is a lineshape function for dispersion related to $\chi_a(\omega)$ by the Kramers–Kronig relations. These are defined as

$$\chi_a(\omega) = \frac{1}{1+\gamma^2(\omega-\omega_0)^2} \text{ and } \chi_d(\omega) = \frac{-(\omega-\omega_0)\gamma}{1+\gamma^2(\omega-\omega_0)^2},$$

where ω_0 is the center and γ is the inverse of the half-width at half-maximum. When using this fit function, f_h is held at the cavity FSR (79.12 MHz), the amplitudes are constrained such that $A_0 > A_1$, and the Doppler profile near the line center is approximated by a third-order polynomial with the quadratic term set to 0.

3.2. H_3^+ Spectra

A sample spectrum of the $R(1,0)$ and $R(1,1)^u$ transitions of the ν_2 fundamental band of H_3^+ is shown in Figure 2. The signals in the top and bottom panels are the demodulated in-phase (black) and quadrature (red, offset) components of the two mixers, which in our setup we measure to be 96° out of phase with one another. The in-phase components of the $R(1,0)$ transition are shown in greater detail in Figure 3. The overall lineshape is slightly asymmetric; the blue side of the transition is stronger than the red side, particularly in mixer 2. The origin of this asymmetry is unknown, and its impact on the spectroscopic accuracy will be discussed below.

A simultaneous fit of the $R(1,0)$ sub-Doppler features in all four detection channels to Eq. (1) is shown in Figure 4. A number of constraints were employed to ensure that the fit parameters were all internally consistent. The line center frequency and Lamb dip width were forced to be equal for all four data channels. Mixers 1 and 2 were held at 96° apart, and the sideband spacing was held equal to the cavity FSR of 79.12 MHz. Because the in-phase and quadrature components of each mixer sample different blends of CM and VM, the Lamb dip amplitudes were allowed to be different for the in-phase channels and the quadrature channels. However, the two in-phase channels were forced to have equal Lamb-dip amplitudes, and likewise for the two quadrature channels. After all of these

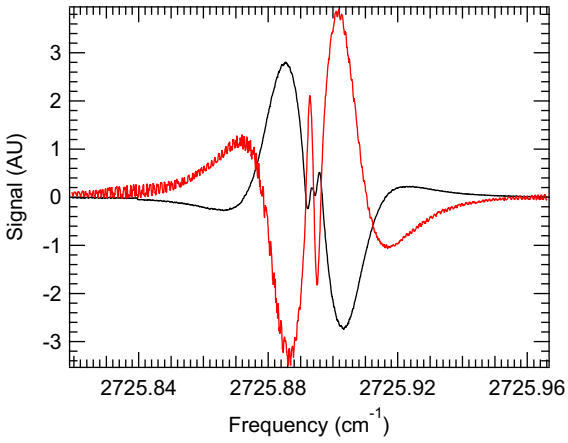

Figure 3. NICE-OHVMS spectrum of the $R(1,0)$ transition of the ν_2 fundamental band of H_3^+. The black trace is the in-phase output of mixer 1, and the red is the in-phase output of mixer 2.

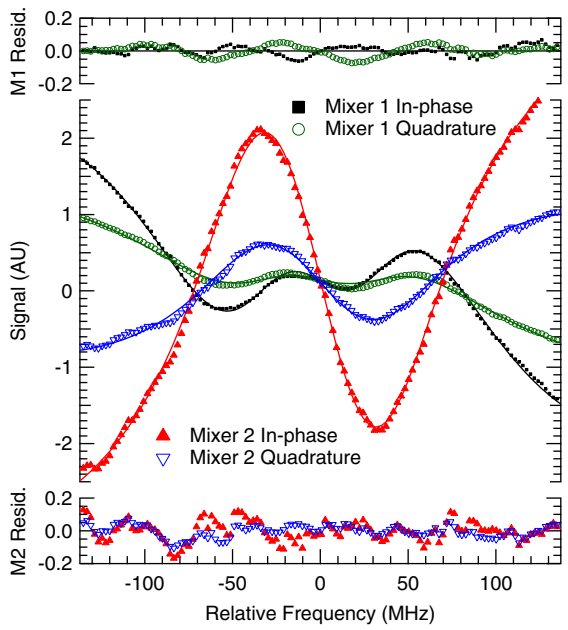

Figure 4. A simultaneous fit of the central sub-Doppler region of the H_3^+ $R(1,0)$ transition from all four data channels to Eq. (1). The symbols in the central portion of the graph are the data, and the solid lines are the fit results. The residuals of the fits are shown in the upper panel for mixer 1 and in the lower panel for mixer 2; in each case the symbols correspond to those in the central panel.

constraints, there are a total of 19 fit parameters for the entire data set: the line center frequency ν_0, the Lamb dip full width at half maximum ($2/\gamma$), the overall detection phase θ_h, Lamb dip amplitudes A_0 and A_1 for the in-phase channels and the quadrature channels, and baseline terms of the form $c_0 + c_1x + c_3x^3$ to approximate the central portion of the Doppler profile in each channel.

The overall quality of the fit is quite good; the residuals are composed primarily of fringing evident on top of the spectrum (especially mixer 2) with the notable exception of the quadrature channel of mixer 1, which has some small systematic deviations on the Lamb dips. The line center ν_0 derived from the fit is $2725.89401954 \pm 0.0000023$ cm^{-1}, but the absolute accuracy is limited by the $> 2 \times 10^{-3}$ cm^{-1} accuracy of the wavemeter, so the exact frequency should not be trusted. More important is the uncertainty of the line center determination, which is $\sim$70 kHz; this represents the maximum potential accuracy of the technique provided suitable frequency calibration is made (but see the discussion

below about the effects of the asymmetry). The overall detection phase θ_h was found to be 132°, indicating a blend of absorption and dispersion in each mixer. Because the Lamb dip widths (full width at half maximum of ~110 MHz as indicated by our fit) are much broader than the Lamb dip spacing of 39.56 MHz ($f_h/2$), the individual Lamb dips for absorption and dispersion cannot be resolved at any RF detection phase. Rather than tuning the phase to separate absorption from dispersion in the two mixers, a phase of 132° was chosen because it was found to isolate the fringing as much as possible in a single detection channel (mixer 2 in-phase), thus minimizing the fringing in the other 3 channels.

4. Discussion

The most interesting aspect of the NICE-OHVMS technique is the presence of Lamb dips which enables high precision measurements of line center frequencies. Prior to the development of NICE-OHVMS, the only methods capable of routine sub-Doppler molecular ion spectroscopy utilized fast ion beams which, due to kinematic compression, give linewidths on the order of 10 to 120 MHz [21–23]. The linewidths from ion beams are comparable to the Lamb dips presented here, though the current work with a positive column has the advantage of much higher ion density than that within an ion beam.

With the H_3^+ Lamb dip linewidths of ~110 MHz demonstrated here, the precision of the line center determination is on the order of 70 kHz. In its present implementation, the technique's accuracy is limited by the wavemeter, and also by slow drifts in the frequency of the signal and idler beams caused by thermal fluctuations of the OPO cavity. Use of an optical frequency comb to stabilize and measure the frequencies of the pump and signal beams would reduce the accuracy uncertainty to < 100 kHz. Ultimately, the total uncertainty of the technique will be determined by the reproducibility of line center determinations once appropriately calibrated.

The asymmetry observed in the overall NICE-OHVMS lineshape can adversely affect the overall accuracy. As mentioned above, the origin of this asymmetry is unknown, although it varies with heterodyne detection phase; similar effects were not observed in the near-IR implementation of NICE-OHVMS [9]. Nevertheless, we have performed simulations of the effects of the asymmetry by synthesizing skewed profiles and comparing the results of our fit function to the actual location of the Lamb dips. Based on the fitting of our simulations, we estimate the magnitude of this line center shifting to be less than a few MHz, even for Doppler profiles that are much more asymmetric than those shown in this Letter. Further study of this phenomenon will be possible with an optical frequency comb, and such work is envisioned in the near future.

The width of the Lamb dips (~110 MHz FWHM from the fitting) is fairly broad. We have varied the intracavity laser power and the cell pressure, but any differences in the linewidth were not observable. However, the ranges of the power and pressure measurements were limited: the intracavity power could only be changed by a factor of 2 before the laser-cavity lock was adversely affected, and the plasma could only give stable operation over 200–600 mTorr. Such wide Lamb dips were also observed in the NICE-OHVMS experiment performed on N_2^+ in the near-IR [9]; in that study, the authors were able to observe a change in linewidth with pressure, but extrapolating to zero pressure still gave a linewidth of ~30 MHz. Assuming that the linewidth is related to the time an ion spends at zero velocity, it is perhaps unsurprising that a less massive ion like H_3^+ has a broader linewidth than N_2^+, as its velocity may be more easily altered by weak long-range interactions.

The fringing apparent in the figures above limits the sensitivity of the present measurements in 2 of the 4 detection channels. The origin of the fringing is not fully understood; however, it appears to have a definite phase with respect to both the heterodyne detection and the plasma modulation. When the plasma is turned off, the fringing does not appear in a scan, and if the cavity transmission detector is blocked while a signal originating from a single fringe is present on a lock-in channel, the signal vanishes. Thus, it appears that the fringing is the result of the plasma interacting with the laser light rather than a purely electronic effect. One possibility is that residual amplitude modulation (RAM) in the heterodyne sidebands is being modulated by the plasma. RAM is an imbalance in the amplitude and/or phase of the sidebands with respect to one another. When demodulated, RAM appears as a DC offset in the heterodyne signal; because of our detection scheme using velocity modulation and $2f$ detection, the NICE-OHVMS would ordinarily be insensitive to such an offset. However, if the refractive index of the plasma varies at $2f$, the DC signal from RAM will be modulated at $2f$ as well, resulting in a net NICE-OHVMS signal. Because RAM is also affected by the presence of etalons in the optical system and the optical frequency, a fringing pattern could possibly result as a function of laser frequency. Testing whether this is truly the origin of the fringing is difficult; however, it is probable that the fringing would be reduced by employing a RAM compensation scheme via temperature and voltage control of the fiber EOM [24].

The sensitivity of the technique at the experimental detection bandwidth of 16 Hz, as determined from the noise-equivalent absorption in the baseline of the in-phase component of mixer 1 (which has the least fringing of the four detection channels), is 3.4×10^{-9} cm^{-1}. which is about two orders of magnitude above the shot noise limit of 3.9×10^{-11} cm^{-1} calculated from

$$\alpha_{\min} = \frac{\pi}{2F}\sqrt{\frac{eB}{\eta P_0}}\frac{1}{J_0(\beta)J_1(\beta)L}, \tag{2}$$

where F is the cavity finesse (120), e the fundamental electric charge, B the detection bandwidth (16 Hz), η the detector responsivity, P_0 the power incident on the detector, $J_n(\beta)$ the nth order Bessel function for modulation index β (0.63), and L the cavity length (190 cm). While NICE-OHMS has been able to achieve a noise level within a factor of 2 of the shot noise limit in one implementation [7], the performance achieved by NICE-OHVMS relative to the shot noise limit is already comparable to a number of other NICE-OHMS setups (see the extensive discussion in Section 4 of [8]).

Ultimately, the absolute sensitivity can be improved by identifying and eliminating noise sources and by increasing the cavity finesse. An increase in cavity finesse leads to additional technical challenge in maintaining the laser-cavity lock, and may make the system even more susceptible to the fringing effects that have already been observed. Such challenges can likely be overcome by improving the bandwidth of the laser frequency corrections (currently limited to the 10 kHz bandwidth of the signal cavity PZT), and correcting for RAM as discussed above.

5. Conclusions

In this Letter, we have demonstrated sub-Doppler spectroscopy of molecular ions in the mid-infrared spectral region using the NICE-OHVMS technique with a cw-OPO. By phase modulating the seed laser with a fiber EOM prior to amplification and optical parametric oscillation, the mid-infrared idler is also phase modulated without requiring a mid-IR EOM. The high optical power of the idler beam allows use of high-bandwidth detectors, which in turn make ultra-sensitive spectroscopy via NICE-OHMS possible. Velocity modulation spectroscopy is then combined with NICE-OHMS to afford ion-neutral discrimination, and the intracavity laser power is sufficient for saturating fundamental rovibrational transitions as demonstrated by spectroscopy of H_3^+. By fitting the sub-Doppler spectral features, the center frequencies of individual rovibrational lines can be measured with a precision of 70 kHz, and the maximum

achieved sensitivity is within a factor of ~90 of the shot noise limit. Improvements to the technique, such as addition of an optical frequency comb for accurate wavelength calibration, technical modifications to improve its sensitivity, and expanding the frequency coverage of the OPO from 3.2–3.9 μm to 2.8–4.8 μm, are envisioned.

The authors thank Takeshi Oka for providing us with the liquid nitrogen cooled plasma cell and its associated pumps and plasma electronics. KNC and BMS acknowledge support from a NASA Earth and Space Science Fellowship. JNH acknowledges support from a Springborn Fellowship and a National Science Foundation Graduate Research Fellowship (DGE 11-44245 FLLW). This work has been supported by the National Science Foundation (PHY 08-55633), the NASA Laboratory Astrophysics program (NNX08AN82G), and a David and Lucile Packard Fellowship.

References

[1] C.S. Gudeman, M.H. Begemann, J. Pfaff, R.J. Saykally, Phys. Rev. Lett. 50 (1983) 727.
[2] C.S. Gudeman, M.H. Begemann, J. Pfaff, R.J. Saykally, J. Chem. Phys. 78 (1983) 5837.
[3] S.K. Stephenson, R.J. Saykally, Chem. Rev. 105 (2005) 3220.
[4] B.M. Siller, A.A. Mills, B.J. McCall, Opt. Lett. 35 (2010) 1266.
[5] A.A. Mills, B.M. Siller, B.J. McCall, Chem. Phys. Lett. 501 (2010) 1.
[6] L.C. Sinclair, K.C. Cossel, T. Coffey, J. Ye, E.A. Cornell, Phys. Rev. Lett. 107 (2011) 093002.
[7] J. Ye, L.-S. Ma, J.L. Hall, J. Opt. Soc. Am. B 15 (1998) 6.
[8] A. Foltynowicz, F. Schmidt, W. Ma, O. Axner, Appl. Phys. B 92 (2008) 313.
[9] B.M. Siller, M.W. Porambo, A.A. Mills, B.J. McCall, Opt. Exp. 19 (2011) 24822.
[10] M.S. Taubman, T.L. Myers, B.D. Cannon, R.M. Williams, Spectrochim. Acta 60 (2004) 3457.
[11] M.W. Porambo, B.M. Siller, J.M. Pearson, B.J. McCall, Opt. Lett., in press.
[12] W.D. Watson, Astrophys. J. 183 (1973) L17.
[13] E. Herbst, W. Klemperer, Astrophys. J. 185 (1973) 505.
[14] T. Oka, Phys. Rev. Lett. 45 (1980) 531.
[15] C.M. Lindsay, B.J. McCall, J. Mol. Spectrosc. 210 (2001) 60.
[16] C.P. Morong, J.L. Gottfried, T. Oka, J. Mol. Spectrosc. 255 (2009) 13.
[17] L. Velilla, B. Lepetit, A. Aguado, J.A. Beswick, M. Paniagua, J. Chem. Phys. 129 (2008) 084307.
[18] C. Lindsay, E.T. White, T. Oka, Chem. Phys. Lett. 328 (2000) 129.
[19] A. Foltynowicz, W. Ma, O. Axner, Opt. Exp. 16 (2008) 14689.
[20] O. Axner, W. Ma, A. Foltynowicz, J. Opt. Soc. Am. B 25 (2008) 1166.
[21] C.S. Gudeman, R.J. Saykally, Ann. Rev. Phys. Chem. 35 (1984) 387.
[22] J.V. Coe, J.C. Owrutsky, E.R. Keim, N.V. Agman, D.C. Hovde, R.J. Saykally, J. Chem. Phys. 90 (1989) 3893.
[23] A.A. Mills, B.M. Siller, M.W. Porambo, M. Perera, H. Kreckel, B.J. McCall, J. Chem. Phys. 135 (2011) 224201.
[24] I. Silander, P. Ehlers, J. Wang, O. Axner, J. Opt. Soc. Am. B 29 (2012) 916

Kyle Crabtree graduated with a B.S. in Chemistry from Ball State University in 2006, and received his Ph.D. in Chemistry from the University of Illinois in 2012. He is currently a CfA Postdoctoral Fellow at the Harvard-Smithsonian Center for Astrophysics.

James Hodges received a B.S. in Chemistry and a B.S. in Polymer & Fiber Chemistry in 2010 from Clemson University. He currently attends the University of Illinois pursuing a PhD in Chemistry as a Springborn Fellow and an NSF Graduate Research Fellow.

Brian Siller graduated with a B.A. in Chemistry, Computer Science, and Mathematics from Ohio Wesleyan University in 2007, and is currently pursuing a Ph.D. in Physical Chemistry at the University of Illinois.

Adam Perry graduated with a B.S. in Chemistry from Oregon State University in 2011, and is currently a graduate student in Physical Chemistry at the University of Illinois.

Joe Kelly graduated with a B.S. in Chemistry from the University of Illinois in 2012.

Paul Jenkins II is currently pursuing his B.S. in Chemical Engineering at the University of Illinois, and plans to graduate in 2015.

Ben McCall received his Ph.D. from the University of Chicago in Chemistry and Astronomy & Astrophysics. Following a Miller Research Fellowship at the University of California at Berkeley, he joined the faculty of the University of Illinois, where he is currently an Associate Professor of Chemistry and Astronomy.